Journal of Engineering Mathematics (2006) 54: 197–210
DOI 10.1007/s10665-006-9030-9

Analytical solution to a sea-water intrusion problem with a fresh water zone tapering to a triple point

A.R. KACIMOV[1,*], Yu.V. OBNOSOV[2], M.M. SHERIF[3] and J.S. PERRET[1]
[1]*Dept. of Soils, Water, and Agricultural Engineering, Sultan Qaboos University, P.O. Box 34, Al-Khod 123, Sultanate of Oman (E-mails: anvar@squ.edu.om; perret@squ.edu.om);* [2]*Institute of Mathematics and Mechanics, Kazan University, University Str., 17, 420008, Kazan, Russia (yobnosov@ksu.ru);* [3]*Department of Civil and Environmental Engineering, United Arab Emirates University, Al-Ain, UAE (msherif@uaeu.ac.ae)*

Received 11 December 2003; accepted in revised form 6 January 2006 / Published online: 23 March 2006

Abstract. A new explicit analytical solution is obtained to a steady-state abrupt interface problem concerning sea-water intrusion into a coastal unconfined homogeneous aquifer with a horizontal impermeable bed and uniformly distributed losses along a phreatic surface. Two free surfaces (encroachment tongue and groundwater table) intersect with a horizontal water table of the resting sea water propagated inland. In the hodograph plane the image of the physical domain is a curvilinear triangle. Conformal mappings of the physical domain and of an unknown complex-potential domain onto an auxiliary half-plane are obtained by a modified method of Polubarinova-Kochina, which is mathematically reduced to a vector Riemann boundary-value problem. Free surfaces are reconstructed for different values of losses, densities of the two fluids, sea water and incident groundwater hydraulic heads. Comparisons with the Dupuit–Forcheimer (hydraulic) model are made and practical implications for catchment-scale groundwater management in Oman and UAE are discussed.

Key words: boundary-value problems, complex potential, hodograph, phreatic surface, sharp interface

1. Hydrological motivation

Sea-water intrusion in coastal aquifers can be caused by overdraft of groundwater through wells ("point sinks"), losses to evapotranspiration from the water table ("distributed sink"), reduced recharge to the water table owing to climatological decline of precipitation or increased runoff over an anthropogenically changing catchment area, rising sea level and sea-water density, among others (the glossary of some hydrological terms is given on our website http://www.squ.edu.om/agr/depts/swae/research/intrusion/index.html). Sea-water tongues encroached into shallow unconfined aquifers have a detrimental impact on plant and crop roots in the soil horizons and on water wells, especially in the arid climates of Oman and UAE [1, 2] where combatting intrusion by hydraulic barriers (*e.g.* polders) is impossible because of the absence of any fresh surface water.

Accurate prediction of intrusion is necessary to implement adequate coastal watershed management strategies, in particular, to mitigate the salinisation damage and to ration pumping. Investigation of horizontal and vertical salinity fields is commonly done by geophysical methods (*e.g.* time-domain electromagnetic sounding and profiling and borehole resistivity measurements). Mathematical models of intrusion are relatively cheap and fast alternatives. They are based on either a variable salinity-density flow (cases 4.2–4.3 from [3]) or abrupt interface flow (case 4.1 from [3]). In this paper we shall study the latter, focusing on a flow

*Corresponding author.

pattern typical for arid conditions which is characterized by low natural replenishment of groundwater and high abstraction rates.

To the best of our knowledge, all sharp interface models mimicking sea-water intrusion in unconfined coastal aquifers (see for example, [4, Figures 9-1, 9-2, 9-5, 9-6, 9-9, 9-11b, 9-12, 9-14, 9-15, 9-16, 9-17, 9-18, 9-19, 9-20, 9-23, 9-30, 9-37]) consider fresh groundwater to be in direct hydraulic contact with the beach slope (horizontal or tilted). In other words, groundwater, at least partially, is postulated to discharge into the sea. This conceptualization implies that a borehole drilled at any proximity to the shore line will first tap a fresh-water zone below which saline water lies under the interface. Consequently, at the corresponding part of the discharging slope (fresh-sea-water contact line) a boundary condition similar to the seepage-face condition in the dam problem holds [5] that in the particular case of a horizontal beach [4, Section 9-3] degenerates into a constant-head condition. "Classical" sharp-interface problems originated from the Ghyben–Herzberg model. It was developed and validated in the humid climates of Holland and Germany. There, the groundwater compartment of the annual hydrological cycle always gains moisture through the water table from the vadose[1] zone compartment. Correspondingly, in most books and papers [4, Figure 9.11], [6, Figure 4.6], [7, Figure 7.10] a phreatic surface is modelled as an isobar with a distributed source (uniform recharge from the vadose zone).

However, in arid countries many shallow aquifers are in completely different conditions of net losses and continuous reduction of storage. For example, in Oman [8] numerous data show that, despite a continuing groundwater flow from the highland part of catchments, no fresh groundwater zone near the shore line is detected and salinity of shallow subsurface water equals or even exceeds [9] that of sea water. In other words, in coastal areas, wells, even through the highest sections of their screens, do not tap any fresh water.

Historical trends [8] indicate also that, in the past, coastal aquifers in Oman and UAE were characterized by "classical" unconfined groundwater-flow patterns with groundwater/sea-water contact at the beach line (sometimes indicated by submarine springs). During the past 30–40 years drilled wells proliferated; electrical pumps have been installed with the main part of pumped water applied for nearby irrigation. On the one hand, sandy soils and sedimentary rock constituting upper coastal aquifers [8] have high conductivity and one can expect a significant percentage of return recharge percolating to the water table. On the other hand, intensive evaporation from the soil surface after watering events not only accumulates salts in the soil profile but also makes the aquifer water balance strongly negative. As a result, sea-water tongues (usually delineated by sharp interfaces) have crept up to 5–6 km inland [8] and are continuing to advance at an alarming rate. For example, in [10] daily intrusion volumes of 140,000 m^3 were reported for a catchment group having a coastal-strip length of 80 km.

Total depletion of fresh water from the coast devastated many agricultural farms that relied on shallow dug wells. Abandoned farms and wells are plentiful in the Batinah area of Oman. When sea water invades and/or soil is salinised, the farm is closed, any groundwater discharge from its area stops but the pumping activity shifts further inland with the piezometric trough and intrusion progressing correspondingly. Coastal towns are more difficult to relocate and potable water is supplied to them in cisterns which are often filled from the highland wells in the same catchment.

Thus, in many coastal arid areas the aquifer input from the mountains is completely intercepted by multiple wells clustered in a progressively shrinking strip. In a plan view, this strip

[1]Vadose refers to the region in the earth's crust just above the permanent groundwater level.

(in Batinah of a width of 5–10 km) is bounded from one side by an advancing saline zone and from another by a geographical limit of agriculturally feasible soil [8].

The main goal of this paper is to study analytically intrusion with a lost contact between groundwater and sea and with a distributed sink condition along a phreatic surface. We will find the free surfaces and investigate the hydrological sustainability of the strip in which fresh groundwater is still available.

2. Conceptual model

We obtain an analytical, 2-D, non-Dupuit-Forchheimer solution to the problem shown in Figure 1 that illustrates a vertical section of a sea-encroached aquifer. We assume steady, 2-D, Darcian, fully saturated unconfined groundwater flow in a homogeneous isotropic aquifer of conductivity k. A fresh-water zone G_z is bounded by the water table AB, with elevation H_f above CU at a distance L from point A. Point A located at a distance L_s from the shore line marks the leftmost upper point of the intrusion zone. The densities of fresh groundwater and sea water, separated from each other by a sharp interface AD, are ρ_f and ρ_s, respectively.

The invaded sea-water zone G_s is stagnant and forms a trapezium $DASU$, side AD of which is curved. We assume that the saline phreatic surface is horizontal and coincides with MSL (mean sea level). AS separates G_s from a dry soil above and the height of the encroached trapezium is H_s. A curved AS would imply that encroached water also moves due to evaporation [11].

Domains G_z and G_s are bounded from below by an impermeable horizontal bedrock.

Line AD in Figure 1 delineates the tongue, the toe of which, D, is a distance l to the left of A. Note that point A is a "triple" point, *i.e.*, a point where the two phreatic surfaces "meet" the interface (or, in other words, where the unsaturated zone contacts fresh and sea water). This point is specific for our conceptual model. A "triple" point was first investigated in [12, pp. 334–340] where canal fresh-water lenses floating on heavier saline indigenous groundwater were studied. Similar hydrodynamic regimes with brine-oil-gas interfaces meeting at a triple point were investigated in [13].

Next, we assume that along the fresh-water phreatic surface AB the losses are distributed uniformly. These losses can be caused by evaporation or capillary rise [14] if the water table is close to the ground surface. On a watershed scale this distributed sink can simulate pumping from G_z if we spread the total pumped quantity over the whole water table. The assumption regarding uniform losses, although not perfect, is necessary for our mathematical technique.

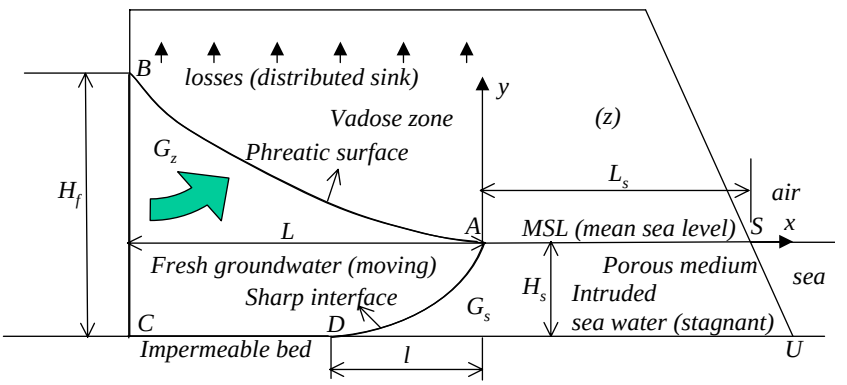

Figure 1. Physical domain.

Mathematically, *AB* and *AD* are two free boundaries, *i.e.*, they are not known *a priori* and should be found as part of the solution along with the distribution of the hydraulic head and Darcian velocity in the flow domain.

In order to corroborate the validity of the flow regime in Figure 1 we dug near-shore pits, collected soil and groundwater samples, monitored regularly the EC (electrical conductance) of water from installed piezometers and conducted a geophysical survey using an OhmMapper TR2. All field data indicate that a sea-water intrusion zone does not occur as a "classical" quasi-triangular tongue [4, Figure 9.11] but is more like a trapezium-type slug completely blocking fresh-water discharge into the sea.

3. Statement of the boundary-value problem

The hydraulic head $h(x, y)$ in G_z is defined as $p/\gamma = h - y$ where p denotes the fresh-water pressure and $\gamma = \rho_f g$ is the specific weight of fresh water. As we work with the gauge pressure and originate our coordinate system at point A in Figure 1, we have $h_A = 0$. Consequently, $h_{BC} = k(H_f - H_s)$ where k is the saturated hydraulic conductivity. We introduce a velocity potential $\Phi = -kh$ and the complex potential $w = \Phi + \mathrm{i}\Psi$, where Ψ is a nondimensional stream function (complex conjugated with Φ), which varies from 0 at point A to Q at point B. The complex-potential domain G_w is shown in Figure 2a. Note that BA is not a streamline; it is depicted schematically in Figure 2a. Note also that from the balance of pressures in the fresh and the sea water at point D we have $\Phi_D = -H_s/\delta$, where $\delta = \rho_f/(\rho_s - \rho_f)$. Consequently, in order to ensure that $x_D > x_C$ the following inequality should hold: $q = (H_f - H_s)/H_s > 1/\delta$. Graphically this means that point D is to the right of point C in G_w (Figure 2a).

According to Darcy's law the specific discharge vector $\vec{V}$ is $\vec{V} = \nabla\Phi$. We introduce also the complex physical coordinate $z = x + \mathrm{i}y$.

Functions Φ and Ψ satisfy the Laplace equation

$$\Delta\Phi(x, y) = 0, \quad \Delta\Psi(x, y) = 0. \tag{1}$$

The boundary conditions for w and z are

$$\begin{array}{llll} \Phi + ky = 0, & \Psi + \varepsilon x = 0 & \text{along} & AB \\ \Phi = -k(H_f - H_s), & x = -L & \text{along} & BC \\ \Psi = 0, & y = -H_s & \text{along} & CD \\ \Phi - cy = 0, & \Psi = 0 & \text{along} & DA \end{array} \tag{2}$$

where the conductivity is $0 < k < \infty$, the rate of losses through AB is $0 < \varepsilon < \infty$, $c = k/\delta$ ($c/k \approx 0{\cdot}03$ in the Gulf of Oman but generally $\varepsilon \le c < \infty$). The first line in (2) adopted from [12, pp. 53–54] states that the losses from G_z are uniformly distributed along AB. This implies, in particular, that $Q = \varepsilon L$. This smeared-losses condition has been used recently in [11, 20]. Capillary fringe is also neglected. The second line in (2) sets a feeding groundwater level in the upper catchment where pumping-evaporation can be neglected (pre-intrusion level). The incident groundwater flow coming through BC is normally unidirectional and obeys well the Dupuit-Forchheimer (DF) model, *i.e.*, BC is indeed an equipotential line. The third line in (2) reflects impermeability of the subjacent bedrock. The fourth line includes the no-flow condition along the interface (we assumed sea water to be stagnant) and continuity of pressure across DA, *i.e.*, no capillary jump exists on this free boundary.

Obviously, in (2) $H_f > H_s > 0$. If $H_s > H_f$, fresh water and interface do not exist and sea water seeps through BC as in [12, pp. 264–280] (a rectangular dam problem). From (2) we

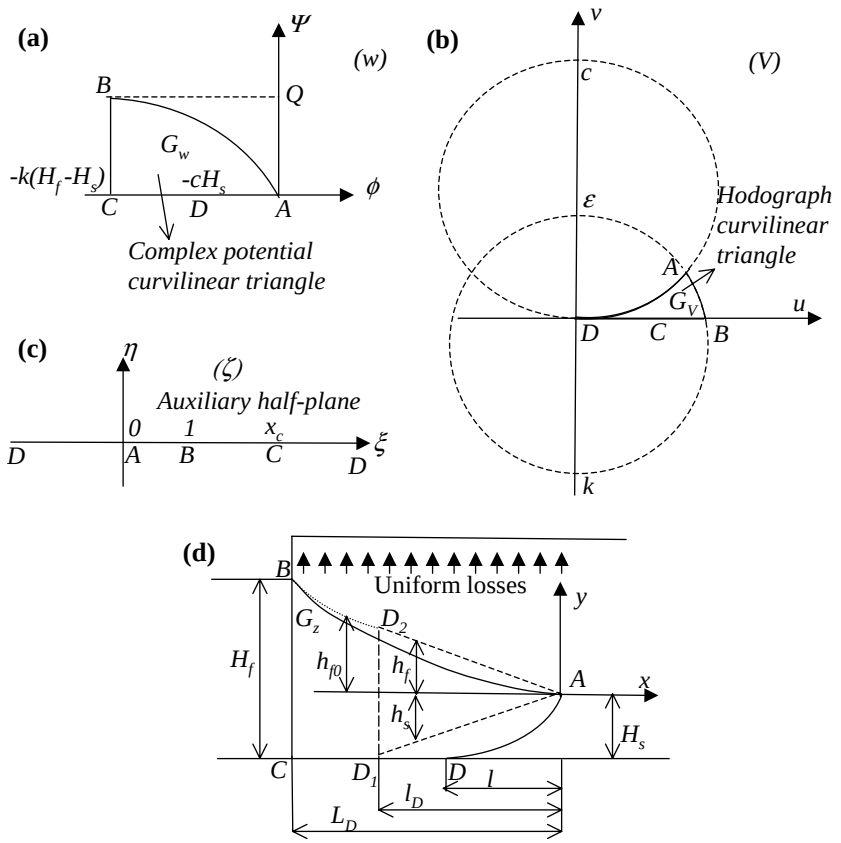

Figure 2. (a) Complex potential domain, (b) hodograph, (c) auxiliary plain, and (d) hydraulic model.

can easily construct the hodograph domain G_V where $V = u + \mathrm{i}v$; here u and v are the horizontal and vertical components of $\vec{V}$. As is shown in Figure 2b, G_V is a curvilinear triangle. From the hodograph we can understand why $\varepsilon \leq c$. If this inequality does not hold, the flow scheme in Figure 1 does not exist.

We denote by $z(\zeta)$ the conformal mapping of the upper half-plane $\zeta > 0$ in an auxiliary plane (Figure 2c) onto G_z with the following correspondence of points $A \to 0$, $B \to 1$, $C \to x_c$, and $D \to \infty$ with an unknown parameter $x_c > 1$. This function has to be found.

Second, we introduce two auxiliary functions

$$F(\zeta) = \mathrm{d}w(\zeta)/\mathrm{d}\zeta, \qquad Z(\zeta) = \mathrm{d}z(\zeta)/\mathrm{d}\,\zeta$$

We can rewrite (2) as

$$\begin{aligned}
&\Im\mathrm{m}[\mathrm{i}\,F + kZ] = \Im\mathrm{m}[F + \mathrm{i}\,\varepsilon Z] = 0 \quad \text{along} \quad AB,\\
&\Im\mathrm{m}[\mathrm{i}\,F] = \Im\mathrm{m}[\mathrm{i}\,Z] = 0 \quad \text{along} \quad BC,\\
&\Im\mathrm{m}F = \Im\mathrm{m}\,Z = 0 \quad \text{along} \quad CD,\\
&\Im\mathrm{m}[\mathrm{i}\,F - cZ] = \Im\mathrm{m}\,F = 0 \quad \text{along} \quad DA.
\end{aligned} \tag{3}$$

The function $\omega = \mathrm{d}\,w/\mathrm{d}\,z = F/Z$ is complex-conjugated with $V = u + \mathrm{i}v$, *i.e.*, $\omega(z)$ is holomorphic and $V(z)$ is antiholomorphic. We have to determine $F(\zeta)$ and $Z(\zeta)$ and then, by integration, reconstruct $z(\zeta)$ and $w(\zeta)$.

4. Solution

As is clear from (3), the problem can be treated by the Polubarinova-Kochina (PK) method that has been recently used in modelling viscous flows, diffusion, and seepage [5, 15–20].

We note that in G_z the angle at point C is 90 degrees because we assumed a vertical constant head line BC and a horizontal bedrock. Similarly, in G_w we have the same angle because BC is an equipotential line and CD is a streamline. Therefore, $F(\zeta)$ and $Z(\zeta)$ can be represented as

$$F(\zeta) = -\mathrm{i}\, F_0(\zeta)/\sqrt{x_c - \zeta}, \quad Z(\zeta) = -\mathrm{i}\, Z_0(\zeta)/\sqrt{x_c - \zeta} \tag{4}$$

with F_0, Z_0 being holomorphic functions at the point x_c. PK calls point C a "removable" singularity.

Let us fix the branch of the radical $\sqrt{x_c - \zeta}$ in the upper half-plane, $\Im\mathrm{m}\,\zeta > 0$, by the condition $-\pi < \arg(x_c - \zeta) < 0$. Now we transform (3) in the auxiliary half-plane as

$$\begin{aligned} &\Im\mathrm{m}[\mathbf{X}K_2] = 0, && -\infty < \xi < 0, \\ &\Im\mathrm{m}[\mathbf{X}K_1] = 0, && 0 < \xi < 1, \\ &\Im\mathrm{m}\,\mathbf{X} = 0, && \xi > 1, \end{aligned} \tag{5}$$

where $\mathbf{X}$ is a vector:

$$\mathbf{X} = (F_0, Z_0) \tag{6}$$

and K_j, $j = 1, 2$ are matrices:

$$K_1 = \begin{Vmatrix} 1 & \mathrm{i} \\ -\mathrm{i}k & -\varepsilon \end{Vmatrix}, \quad K_2 = \begin{Vmatrix} 1 & \mathrm{i} \\ \mathrm{i}c & 0 \end{Vmatrix} \tag{7}$$

Because of (5), the vector-function

$$\mathbf{U}(\zeta) = \begin{cases} \mathbf{X}(\zeta), & \Im\mathrm{m}\,\zeta > 0 \\ \overline{\mathbf{X}(\bar{\zeta})}\,\overline{K}_2 K_2^{-1}, & \Im\mathrm{m}\,\zeta < 0 \end{cases} \tag{8}$$

is the analytical continuation of the function (6) into the lower half-plane through the half-axis $(-\infty, 0)$ (an overbar means complex conjugation). Our vector function satisfies the conditions:

$$\begin{aligned} &\mathbf{U}^+(\xi) = \mathbf{U}^-(\xi), && \xi < 0 \\ &\mathbf{U}^+(\xi) = \mathbf{U}^-(\xi) T_1, && 0 < \xi < 1; \quad \mathbf{U}^+(\xi) = \mathbf{U}^-(\xi) T_2, \quad \xi > 1 \end{aligned} \tag{9}$$

where

$$\begin{aligned} T_1 &= K_2 \overline{K}_2^{-1} \overline{K}_1 K_1^{-1} = \tfrac{1}{k+\varepsilon} \begin{Vmatrix} k - \varepsilon - 4k\varepsilon/c & -2\mathrm{i}(c - \varepsilon + k)/c \\ -2\mathrm{i}\,k\varepsilon & k - \varepsilon \end{Vmatrix}, \\ T_2 &= K_2 \overline{K}_2^{-1} = \begin{Vmatrix} -1 & 2\mathrm{i}/c \\ 0 & -1 \end{Vmatrix}. \end{aligned} \tag{10}$$

Besides, from (8) the solution of problem (9) has to satisfy the symmetry condition

$$\overline{\mathbf{U}(\bar{\zeta})\, T_2} \equiv \mathbf{U}(\zeta) \tag{11}$$

We look for a solution of problem (9), (11). This solution integrable singularities at the points $0, 1$ and ∞.

Thus, we have arrived at the well-known Riemann boundary-value problem (9) for a two-dimensional vector function (6) with a piece-wise constant coefficient [21, 22]. We find the exponents of singularities at the points $\zeta=0$, $\zeta=1$ and $\zeta=\infty$ by a modified PK method. Namely, it is easy to prove that the exponents are equal to the arguments, divided by 2π, of the eigenvalues of matrices T_1, $T_1^{-1}T_2$, and T_2^{-1}. It is convenient to take the required eigenvalues as $\lambda_1=\overline{\lambda_2}=\exp[\mathrm{i}\,2\pi(1/2-\alpha)]$, $\lambda_3=\overline{\lambda_4}=\exp[\mathrm{i}\,2\pi(1/2-\beta)]$, and $\lambda_5=\lambda_6=-1$, which are the eigenvalues of the matrix T_1, $T_1^{-1}T_2$, and T_2^{-1}, correspondingly. Here

$$2\pi\alpha=\arccos\frac{\varepsilon-k+2k\varepsilon/c}{k+\varepsilon},\qquad 2\pi\beta=\arccos\frac{k-\varepsilon}{k+\varepsilon} \tag{12}$$

are the internal angles at the vertices A, B of the curvilinear triangle ABD in Figure 2c. Accordingly, the exponents are $\pm(1/2-\alpha)$ at the point $\zeta=0$ and $\pm(1/2-\beta)$, $1/2$ at the points $\zeta=1$, $\zeta=\infty$, respectively.

Let us consider now the Riemann P-function

$$\begin{aligned}
&P\begin{pmatrix} 0 & 1 & \infty \\ \alpha-1/2 & \beta-1/2 & 3/2\,;\zeta \\ -\alpha-1/2 & -\beta-1/2 & 3/2 \end{pmatrix} \\
&=\zeta^{\alpha-1/2}(1-\zeta)^{\beta-1/2}P\begin{pmatrix} 0 & 1 & \infty \\ 0 & 0 & 1/2+\alpha+\beta\,;\zeta \\ -2\alpha & -2\beta & 1/2+\alpha+\beta \end{pmatrix} \\
&=\zeta^{\alpha-1/2}(1-\zeta)^{\beta-1/2}\mathrm{F}(1/2+\alpha+\beta,\,1/2+\alpha+\beta;\,1+2\alpha;\,\zeta),
\end{aligned}$$

where $\mathrm{F}(p,q;r;\zeta)$ is the hypergeometric function.

The components of the Riemann P-function differ from the found exponents in integers. If these components were equal to the exponents, then one would arrive at the solution of the problem (9) with only one component having $\zeta=0$ and $\zeta=1$ as singular points and another component would be bounded at these points. We note that the PK method adds a certain integer to the exponent to match the behaviour of the pair of searched functions at the three singular points. Qualitatively, this behaviour can be retrieved directly from the corresponding domains in the physical plane and hodograph. The choice of the components of the P-function depends on the conformal mapping determined by $w(\zeta)$ and $z(\zeta)$. From Figure 1 and Figure 2a we can infer that the derivatives of these two functions can not be bounded at $\zeta=0$ and $\zeta=1$, *i.e.*, $w'(\zeta)$ and $z'(\zeta)$ have integrable singularities there. As regards the third singular point $\zeta=\infty$, from Figure 2a we can see that F_0 behaves there as $\sim\zeta^{-3/2}$. From Figure 2b we can see that Z_0 at infinity behaves as $\sim\zeta^{-3/2}\log\zeta$.

The above hypergeometric function is a solution of the hypergeometric equation

$$\zeta(1-\zeta)Y''+[1+2\alpha-2(1+\alpha+\beta)\zeta]Y'-(1/2+\alpha+\beta)^2Y=0.$$

This equation has another solution $\zeta^{-2\alpha}\mathrm{F}(1/2-\alpha+\beta,\,1/2-\alpha+\beta;\,1-2\alpha;\,\zeta)$, which is linearly independent of the first one. Both these solutions are defined in the disk $|\zeta|<1$. We denote

$$Y_{1(0)}=(1-\zeta)^{\beta-1/2}\,f(\zeta;\alpha,\beta),\qquad Y_{2(0)}=(1-\zeta)^{\beta-1/2}\,f(\zeta;-\alpha,\beta), \tag{13}$$

where

$$f(\zeta;\alpha,\beta)=\mathrm{B}\left(\frac{1}{2}+\alpha+\beta,\,\frac{1}{2}+\alpha-\beta\right)(-\zeta)^{\alpha-1/2}\mathrm{F}\left(\frac{1}{2}+\alpha+\beta,\,\frac{1}{2}+\alpha+\beta;\,1+2\alpha;\,\zeta\right)$$

The multiplier in the last expression (the Beta-function, $\mathrm{B}(x,y)$) is factored out to simplify the following evaluations. The branches of the functions $(-\zeta)^{\nu}$ and $(1-\zeta)^{\mu}$ are fixed in $C\setminus(0,\infty)$

and $C\setminus(1,\infty)$ by the conditions $|\arg(-\zeta)|<\pi$ and $|\arg(1-\zeta)|<\pi$, respectively. The functions fixed in this manner satisfy the same symmetry condition $f(\zeta)\equiv\overline{f(\bar{\zeta})}$. Hence, both functions (13) satisfy the same symmetry condition too.

Now we look for the components of the unknown vector (8) that constitute a linear combination of functions (13), *i.e.*,

$$\mathbf{U}=(Y_1,Y_2)C_0=\mathbf{Y}C_0, \tag{14}$$

where $Y_j=Y_{j(0)}$, $j=1,2$, in the vicinity of zero and C_0 is a 2×2 constant matrix:

$$C_0=\begin{Vmatrix} c_{11} & c_{12} \\ c_{21} & c_{22} \end{Vmatrix},$$

which components c_{ij} have to be determined from the boundary conditions (9) and symmetry condition (11).

It can be easily proved that, if a function $\mathbf{U}(\zeta)$ is a solution of the problem (9), then $\overline{\mathbf{U}(\bar{\zeta})T_2}$, as well as

$$\mathbf{U}(\zeta)+\overline{\mathbf{U}(\bar{\zeta})T_2}, \tag{15}$$

are solutions of the same problem and (15) meets the symmetry condition (11).

Invoking (9), (13), (14), we get for $0<\xi<1$:

$$\mathbf{U}^+(\xi)=\mathbf{Y}^+C_0,\quad \mathbf{U}^-(\xi)=\mathbf{Y}^+\mathrm{diag}(\mathrm{e}^{-\mathrm{i}2\pi(1/2-\alpha)},\mathrm{e}^{\mathrm{i}2\pi(1/2-\alpha)})C_0$$

Hence, the function (14) satisfies the first of the boundary conditions (9) if

$$\mathrm{diag}(\mathrm{e}^{\mathrm{i}2\pi(1/2-\alpha)},\mathrm{e}^{-\mathrm{i}2\pi(1/2-\alpha)})=C_0T_1C_0^{-1}.$$

Consequently, after some algebra, we derive

$$C_0=\mathrm{diag}(c_1,c_2)\begin{Vmatrix} -a\bar{\lambda} & -\mathrm{i}\,b\lambda \\ a\lambda & \mathrm{i}\,b\bar{\lambda} \end{Vmatrix} \tag{16}$$

where the unknown complex components c_1, c_2 are to be defined later, and

$$a=\sqrt{\varepsilon k c},\quad b=\sqrt{c-\varepsilon+k},\quad \lambda^2=\frac{\sqrt{\varepsilon k}+\mathrm{i}\sqrt{(c-\varepsilon)(c+k)}}{\sqrt{c(c-\varepsilon+k)}}. \tag{17}$$

To check the second condition in (9) we have to continue the hypergeometric functions in (13) into the vicinity of $\zeta=\infty$. The needed analytical continuation is ([23, Equation 15.3.13])

$$\begin{aligned} Y_{1(\infty)}&=(-\zeta)^{-\beta-1}(1-\zeta)^{\beta-1/2}\sum_{n=0}^{\infty}\frac{\left(\frac{1}{2}+\alpha+\beta\right)_n\left(\frac{1}{2}-\alpha+\beta\right)_n}{(n!)^2}\zeta^{-n}\left(h_n+\ln(-\zeta)\right), \\ Y_{2(\infty)}&=Y_{1(\infty)}+hY_\infty, \end{aligned} \tag{18}$$

where $(p)_q=\Gamma(p+q)/\Gamma(q)$, and $\Gamma(\cdot)$ is the Gamma function,

$$Y_\infty=(-\zeta)^{-\beta-1}(1-\zeta)^{\beta-1/2}\mathrm{F}(1/2+\alpha+\beta,1/2-\alpha+\beta;1;1/\zeta). \tag{19}$$

The constant $h=h'_n-h_n$ in (18) is

$$\begin{aligned} h_n&=2\psi(n+1)-\psi(\tfrac{1}{2}+\alpha+\beta+n)-\psi(\tfrac{1}{2}+\alpha-\beta-n), \\ h'_n&=2\psi(n+1)-\psi(\tfrac{1}{2}-\alpha+\beta+n)-\psi(\tfrac{1}{2}-\alpha-\beta-n), \end{aligned} \tag{20}$$

where $\psi(\zeta)$ is the Psi function. Note that the difference $h = h'_n - h_n$ does not depend on n. Indeed, using [24, Equation 6.358.8] and (20), (12), we get

$$h = \pi\,(\tan\pi(\alpha-\beta)+\tan\pi(\alpha+\beta)) = \frac{2\pi\sqrt{(c-\varepsilon)(c+k)}}{\sqrt{\varepsilon k}}. \tag{21}$$

For $1<\xi$ we have $Y_j = Y_{j(\infty)}$, $j=1,2$. Then from the second condition (9) and (18)–(21) it follows

$$\mathbf{Y}^+ C_0 = \left(-\mathbf{Y}^+ - 2\pi|Y_\infty|(1,1)\right) C_0 T_2$$

or

$$\mathbf{Y}^+ C_0 (E+T_2) = -2\pi|Y_\infty|(1,1) C_0 T_2$$

and hence

$$\frac{a2\mathrm{i}}{c}\mathbf{Y}^+ \begin{Vmatrix} 0 & -\overline{\lambda}c_1 \\ 0 & \lambda c_2 \end{Vmatrix} = -2\pi|Y_\infty|(1,1) C_0 T_2.$$

It is not difficult to show now that the last equality holds if and only if $c_1 = R\lambda$, $c_2 = R\overline{\lambda}$ for arbitrary R.

Thus, we have found the following solution of problem (9):

$$\mathbf{U}(\zeta) = R\mathbf{Y} \begin{Vmatrix} -a & -\mathrm{i}\,b\lambda^2 \\ a & \mathrm{i}\,b\overline{\lambda}^2 \end{Vmatrix}.$$

The solution to (9), which satisfies the symmetry condition (11), based on (14) and (15) is

$$\mathbf{U}(\zeta) = \mathbf{Y} \begin{Vmatrix} a(\overline{R}-R) & -\mathrm{i}\,b(\lambda^2 R + \overline{\lambda^2 R}) + 2\mathrm{i}\,a\overline{R}/c \\ -a(\overline{R}-R) & \mathrm{i}\,b(\overline{\lambda}^2 R + \lambda^2\overline{R}) - 2\mathrm{i}\,a\overline{R}/c \end{Vmatrix}. \tag{22}$$

Using the representations (4), (6) we get after some algebra

$$\begin{aligned} F(\zeta) &= a(\overline{R}-R)(Y_1-Y_2)/(\mathrm{i}\sqrt{x_c-\zeta}), \\ Z(\zeta) &= \frac{2}{\sqrt{x_c-\zeta}}\left[\frac{a}{c}\overline{R}(Y_1-Y_2) - b\left(\mathfrak{Re}(\lambda^2 R)Y_1 - \mathfrak{Re}(\overline{\lambda}^2 R)Y_2\right)\right]. \end{aligned} \tag{23}$$

We set $R = r\mathrm{e}^{\mathrm{i}\varphi}$; then from (23) one can conclude that both functions F and Z depend on the imaginary part of R only. According to the last remark, taking $R = \mathrm{i}r$ with an arbitrary real r, we get

$$\begin{aligned} F(\zeta) &= -r\sqrt{\varepsilon k c}(Y_1-Y_2)/\sqrt{x_c-\zeta}, \\ Z(\zeta) &= r\sqrt{\frac{\varepsilon k}{c}}\left[\frac{\sqrt{(c-\varepsilon)(c+k)}}{\sqrt{\varepsilon k}}\frac{(Y_1+Y_2)}{\sqrt{x_c-\zeta}} - \mathrm{i}\,\frac{(Y_1-Y_2)}{\sqrt{x_c-\zeta}}\right]. \end{aligned} \tag{24}$$

Accordingly,

$$\omega(\zeta) = \frac{F}{Z} = -\mathrm{i}\,c\left[1+\mathrm{i}\,\frac{h}{2\pi}\frac{Y_1+Y_2}{Y_1-Y_2}\right]^{-1}$$

with the constant h being defined in (21).

Both functions in (24) have the point $\zeta = 1$ as a singular point. Calculations in the vicinity of this point can be performed using the analytical continuation into the region $|\zeta-1|<1$, $\mathfrak{Im}\,\zeta > 0$ [23, Equation 15.3.6]:

$$
\begin{aligned}
Y_{1(1)} &= (-\zeta)^{\alpha-1/2}\{\gamma(\alpha,\beta)\, f_1(\zeta;\alpha,\beta)+\gamma(\alpha,-\beta)\, f_1(\zeta;\alpha,-\beta)\},\\
Y_{2(1)} &= (-\zeta)^{\alpha-1/2}\mathrm{e}^{\mathrm{i}2\pi\alpha}\{\gamma(-\alpha,\beta)\, f_1(\zeta;\alpha,\beta)+\gamma(-\alpha,-\beta)\, f_1(\zeta;\alpha,-\beta)\},
\end{aligned}
\tag{25}
$$

where

$$
\begin{aligned}
&\gamma(\alpha,\beta) = \mathrm{B}(-2\beta, 1/2+\alpha+\beta),\\
&f_1(\zeta;\alpha,\beta) = (1-\zeta)^{\beta-1/2}\mathrm{F}(1/2+\alpha+\beta, 1/2+\alpha+\beta; 1+2\beta; 1-\zeta).
\end{aligned}
$$

Our solution (24) contains two real parameters r and $x_c > 1$ which can be determined from physical conditions. For example, we can fix the location of point B in G_z, *i.e.*, the constants L and $H_f - H_s$ or the coordinates of point D (l and H_s). Here we shall fix $H_f - H_s$ and H_s. Then r and x_c are determined from the following system:

$$
\begin{aligned}
r\sqrt{\varepsilon k c}\, I_1 &= \int_0^1 \Re\mathfrak{e}[F(\xi)]\,\mathrm{d}\xi = r\sqrt{\varepsilon k c}\int_0^1 \frac{\Re\mathfrak{e}[Y_2(\xi)-Y_1(\xi)]}{\sqrt{x_c-\xi}}\,\mathrm{d}\xi = -k(H_f-H_s),\\
r\sqrt{\frac{\varepsilon k}{c}}\, I_2 &= \int_{-\infty}^0 \Im\mathfrak{m}[Z(\xi)]\,\mathrm{d}\xi = r\sqrt{\frac{\varepsilon k}{c}}\int_{-\infty}^0 \frac{Y_2(\xi)-Y_1(\xi)}{\sqrt{x_c-\xi}}\,\mathrm{d}\xi = H_s.
\end{aligned}
\tag{26}
$$

In accordance with (13), (25), (18) the integrals I_1, I_2 can be written as

$$
\begin{aligned}
I_1 &= \int_0^{0.5} \frac{\Re\mathfrak{e}[Y_{2(0)}(\xi)-Y_{1(0)}(\xi)]}{\sqrt{x_c-\xi}}\,\mathrm{d}\xi + \int_{0.5}^1 \frac{\Re\mathfrak{e}[Y_{2(1)}(\xi)-Y_{1(1)}(\xi)]}{\sqrt{x_c-\xi}}\,\mathrm{d}\xi,\\
I_2 &= h\int_{-\infty}^{-1} \frac{Y_\infty(\xi)}{\sqrt{x_c-\xi}}\,\mathrm{d}\xi + \int_{-1}^0 \frac{Y_{2(0)}(\xi)-Y_{1(0)}(\xi)}{\sqrt{x_c-\xi}}\,\mathrm{d}\xi.
\end{aligned}
$$

Note that according to (18), (19)

$$
\int_{-\infty}^{-1} \frac{Y_\infty(\xi)}{\sqrt{x_c-\xi}}\,\mathrm{d}\xi = \int_{-1}^0 \frac{(1-\xi)^{\beta-1/2}}{\sqrt{1-x_c\xi}}\,\mathrm{F}(1/2+\alpha+\beta, 1/2-\alpha+\beta; 1; \xi)\,\mathrm{d}\xi.
$$

From here we get a nonlinear equation $cI_1/I_2 = kq$ (recall that $q = H_f/H_s - 1$) from which we determined x_c by the *Mathematica* routine `FindRoot` [25, pp. 692–695]. The found value of x_c we put into one of the equations of the system (26) and calculated r. Eventually we used the `ParametricPlot` routine of *Mathematica* [25, p. 167] to calculate both free surfaces as parametric plots based on:

$$
x^* = \frac{x}{H_s} = \frac{1}{I_2}\Re\mathfrak{e}\int_0^\zeta Z(\zeta)\mathrm{d}\zeta, \qquad y^* = \frac{y}{H_s} = \frac{1}{I_2}\Re\mathfrak{e}\int_0^\zeta Z(\zeta)\mathrm{d}\zeta.
$$

In particular, the tongue sizes are:

$$
\begin{aligned}
l^* &= \sqrt{\frac{(c-\varepsilon)(c+k)}{\varepsilon k}}\int_{-1}^0 \left[\frac{Y_{1(0)}(\xi)+Y_{2(0)}(\xi)}{\sqrt{x_c-\xi}} + (-\xi)^{-3/2}\frac{Y_{1(\infty)}(1/\xi)+Y_{2(\infty)}(1/\xi)}{\sqrt{1-x_c\xi}}\right]\mathrm{d}\xi,\\
L^* &= \sqrt{\frac{(c-\varepsilon)(c+k)}{\varepsilon k}}\int_0^1 \frac{Y_1(\xi)+Y_2(\xi)}{\sqrt{x_c-\xi}}\,\mathrm{d}\xi.
\end{aligned}
\tag{27}
$$

We note that an alternative method based on the reference function [26] can be implemented.

5. Results, hydraulic model and conclusion

We fixed $1/\delta = 0{\cdot}03$ (the value relevant to the Gulf of Oman) and plotted the phreatic surface and sharp interface for $q = (H_f - H_s)/H_s = 0{\cdot}1$, $\varepsilon/k = 0{\cdot}015, 0{\cdot}02, 0{\cdot}025$ (Figure 3, curve pairs 1–3, correspondingly). These values of q and ε/k were selected based on typical hydrogeological data from [1, 10] and our own experiments and field studies in the vadose zone.

Dropping the superscripts in (27) we plotted in Figure 4 $L(q)$ and $l(q)$ (curves 1 and 2, respectively) for $\varepsilon/k = 0{\cdot}02$. Figure 5 shows L, l and $L - l$ as functions of ε plotted for $q = 0{\cdot}1$ (curves 1–3, correspondingly).

We note that, although our physical coordinates are originated at point A and we obtained L for BC, practically $L + L_s$ (Figure 1a) is fixed and A should be found from our solution, *i.e.*, both A and D are *a priori* unknown fronts of the free surface (AD).

As Figures 3 and 5 show, for increasing ε the fresh-water strip (L) and its part where any well can be screened up to the bedrock, ($L - l$) shrinks. Based on our conceptual model in Figure 1 it implies further propagation of the encroached saline trapezium.

An increase of q (*i.e.*, H_f) according to Figure 4 results in a practically linear increase of L and no changes in l. Hydrologically it means sweeping of the propagated tongue back to the shore line by increasing the acting head. In Oman and UAE this has been achieved by artificial recharge of unconfined aquifers from retention dams that intercept runoff, generate groundwater mounds and maintain higher H_f than in unreplenished conditions [2, 10].

Now we compare our hydrodynamic (potential) solution with the hydraulic (DF) approximation, which is, according to [4, p. 76], "the only simple tool available to most engineers and hydrologists" (see also [6, 7]). Such comparisons are important to test the accuracy of hydraulic models (*e.g.*, [12, Chapter 10], [27]) against the potential model and the sharp interface model against variable density-salinity ones [3, cases 4.2–4.3].

We divide our flow (Figure 1d) into zones D_1D_2A (zone 1) and CBD_2D_1 (zone 2) such that D_1 is the tip of the DF interface located at a distance l_D from the triple point ($l_D \neq l$). We introduce the discharge potential Φ_d according to [6, pp. 108–112]. This potential satisfies the governing equation

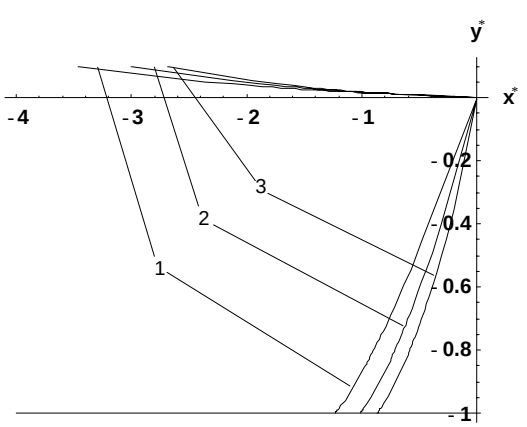

Figure 3. Phreatic surface (upper curve) and sharp interface (lower curve) in hydrodynamic model for $q = 0{\cdot}1$, $\varepsilon/k = 0{\cdot}015, 0{\cdot}02, 0{\cdot}025$.

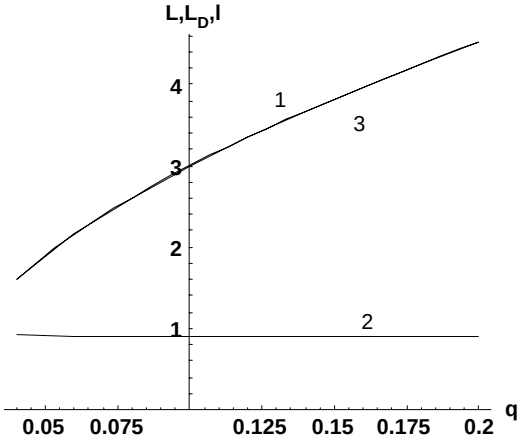

Figure 4. Fresh-water zone length L (curve 1) in hydrodynamic model, tongue length l (curve 2) and fresh-water zone length in hydraulic model L_D (curve 3) as functions of q for $\varepsilon/k = 0{\cdot}02$.

$$\frac{d^2\Phi_D}{dx^2}=\varepsilon, \quad \text{on } -L\le x\le 0, \tag{28}$$

where

$$\Phi_D=k(h_f+h_s)^2/2, \quad \text{on } -l_D\le x\le 0,$$
$$\Phi_D=k(h_{f0}+H_S)^2/2, \quad \text{on } -L\le x\le -l_D,$$

where $h_f(x)$ is the height of the DF water table above MSL in AD_1D_2, $h_s(x)$ is the depth of the interface below MSL ($h_f, h_s>0$) and $h_{f0}(x)$ is the height of the DF water table in BD_2D_1C.

According to a standard set of DF assumptions, the pressure is hydrostatic both in the moving groundwater and stagnant sea water and therefore $h_s=\delta h_f$. We integrate (28) once in the interval $-l_D<x<0$ and get $-Q_{DF}(x)=k(h_f+h_s)\,dh_f/dx=\varepsilon x+c_1$ where Q_{DF} is the flow rate above the interface, which decreases from Q_0 along D_1D_2 to 0 at point A. Therefore, the first constant of integration is $c_1=0$. A second integration yields $k(1+\delta)h_f^2=\varepsilon x^2+c_2$. The second constant of integration is $c_2=0$ because $h_f(0)=0$. Eventually, the DF phreatic surface and interface in zone 1 are described by:

$$h_f=-\sqrt{\frac{\varepsilon}{k(1+\delta)}}x, \qquad h_s=\delta h_f, \qquad l_D=\frac{H_s}{\delta}\sqrt{\frac{1+\delta}{\varepsilon/k}}. \tag{29}$$

Equation (29) complements the catalogue of straight phreatic surface-interface solutions [18, 28]. Thus, the fragment AD_1D_2 is a triangle (Figure 2d).

In zone 2 Equation (28) is integrated analogously, giving a hyperbolic water table

$$h_{f0}+H_s=\sqrt{\frac{\varepsilon}{k}x^2+c_3x+c_4}.$$

The integration constant c_3 is found from the condition that at cross-section D_1D_2 the flow rate Q_{DF} between two zones is continuous and equals $Q_0=\varepsilon l_D$. This immediately gives $c_3=0$. The constant c_4 is found from the condition that the hyperbolic and straight limbs of

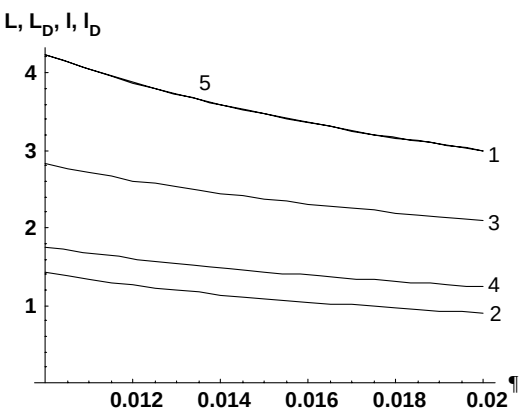

Figure 5. Flow-domain dimensions L, l and $L-l$ (curves 1-3) in hydrodynamic model and l_D, L_D (curves 4, 5) in hydraulic model as functions of ε at $q=0{\cdot}1$.

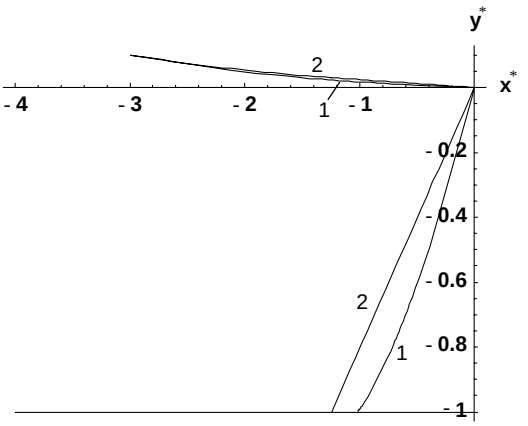

Figure 6. Water table and sharp interface for $q=0{\cdot}1$, $\varepsilon/k=0{\cdot}02$ according to the potential (curve pairs 1) and DF (curve pairs 2) models.

the water table coincide at point D_2 which results in $c_4 = H_s^2(1+\delta)/\delta$. Finally we obtain for BD_2

$$h_{f0} = \sqrt{\frac{\varepsilon}{k}x^2 + H_s^2\frac{1+\delta}{\delta}} - H_s. \tag{30}$$

The water table elevation at point B is $H_f - H_s$, which upon substitution in (30) gives

$$L_D^* = \frac{L_D}{H_s} = \sqrt{\frac{H_f^2}{H_s^2} - \frac{1+\delta}{\delta}}\Big/\sqrt{\frac{\varepsilon}{k}}. \tag{31}$$

From (31) we see that the DF problem is solvable if $H_f/H_s > \sqrt{(1+\delta)/\delta}$. This condition (similarly to one in the full potential model) states that water moves from left to right in Figure 2d.

In Figure 6 we show the water table and interface for $q = 0{\cdot}1$, $\varepsilon/k = 0{\cdot}02$ calculated from the potential (curves 1) and DF (curves 2) models. In Figure 4 (curve 3) we plot $L_D(q)$ from (31). This curve can hardly be discerned from $L(q)$ in the potential model. We note that, according to (29), $l_D \approx 1{\cdot}243$, which is higher than l. The DF sizes l_D and L_D are also shown in Figure 5 as functions of ε/k (curves 4 and 5). As we can see, curve 5 is nearly identical with L obtained from the potential model, while curve 4 is somewhat higher than l.

Overall, the DF model gives a reasonable prediction of the interface and water table and we extended this model to the catchment scale hydrologic systems [29–30]. If the aquifer thickness is much larger than its height (*e.g.*, in the coastal zones of Oman and UAE, common height-to-length ratios are $\sim(50, 600)\text{m}/(5-50)\text{km}$ [2, 8]) then, instead of the hydrodynamic equation (27), one can use its simple hydraulic alternatives (29) and (31), which can be more easily comprehended (*e.g.* from (31), and one can immediately see that $L_D \sim 1/\sqrt{\varepsilon}$).

Thus, we implemented the Polubarinova-Kochina technique to tackle a new boundary-value problem, which is mathematically reduced to the reconstruction of two holomorphic functions in a domain having a phreatic surface and an abrupt interface between fresh and saline water. The imaginary and real parts of the functions form a linear combination along the boundaries of the flow domain. We obtained a rigorous analytical solution which is computationally reduced to a numerical integration of hypergeometric functions. This solution is compared with a DF solution which gives a straight interface and a water table consisting of a straight line concatenated with a hyperbola. The effect of the intensity of a distributed sink (evaporation or spread pumping), density contrast, mean sea level and hydraulic head in the highland area feeding a coastal aquifer on the shape of the free surfaces has been investigated.

Acknowledgements

This study was supported by the joint Sultan Qaboos University – United Arab Emirates University collaboration project CL/SQU-UAEU/0/3/02 and by the Russian Foundation for Basic Research the regional grant 03-01-96193-r2003tatarstan_a. Comments and criticism of four anonymous referees, Prof. Kuiken and helpful discussions with A.Al-Mushikhi and S.Al-Obaidani are appreciated.

References

1. *Sea Water Intrusion Beneath the Batinah Coast, 1983–1995.* Sultanate of Oman Ministry of Water Resources. Muscat: International Printing Press (1996).
2. *Wadi Bih Dam and Groundwater Recharge Facilities, Volume I Design.* Electrowatt Engineering Services Ltd. Ministry of Agriculture and Fisheries, UAE (1981).

3. G. Segol, *Classic Groundwater Simulations: Proving and Improving Numerical Models*. Englewood Cliffs: Prentice Hall (1994) 531 pp.
4. J. Bear, *Hydraulics of Groundwater*. NewYork: McGraw-Hill (1979) 567 pp.
5. A.R. Kacimov and Yu.V. Obnosov, Analytical solution for a sharp interface problem in sea water intrusion into a coastal aquifer. *Proc. R. Soc. London A* 457 (2001) 3023–3038.
6. O.D.L. Strack, *Groundwater Mechanics*. Englewood Cliffs: Prentice Hall (1989) 732 pp.
7. A. Verruijt, *Theory of Groundwater Flow*. London: Macmillan (1982) 144 pp.
8. *Eastern Batinah Resource Assessment. Progress Report N1*. Sultanate of Oman Ministry of Water Resources (1995).
9. Y. Yechieli and W.W. Wood, Hydrogeologic processes in saline systems: playas, sabkhas, and saline lakes. *Earth-Science Rev.* 58 (2002) 343–365.
10. A.A.M. Al-Mushikhi, *Formation of Subsurface Water of the East-south Batinah Region (Sultanate of Oman) and Perspectives of Development*. PhD thesis, Moscow: Moscow State Geoexploration University. (2002) (in Russian) 146 pp.
11. A.R. Kacimov and E.G. Youngs, Steady-state water-table depressions caused by evaporation in lands overlying a water-bearing substratum. *J. Hydrol. Eng. ASCE* 10 (2005) 295–301.
12. P.Ya. Polubarinova-Kochina, *Theory of Ground-Water Movement*. Moscow: Nauka (1977) (in Russian) 664 pp.
13. A.R. Kacimov and Yu.V. Obnosov, Analytical solutions to hydrodynamic problems for oil and gas traps. *J. Hydrol.* 254 (2001) 33–46.
14. E.G. Youngs, Maintaining fresh-water aquifers over saline water in coastal aquifers. *Sultan Qaboos Univ. J. Agricult. Sci.* 7 (2002) 23–28.
15. S.D. Howison and J.R. King, Explicit solutions to six free-boundary problems in fluid flow and diffusion. *IMA J. Appl. Math.* 42 (1989) 155–175.
16. M. Bakker, Groundwater flow with free boundaries using the hodograph method. *Adv. Water Res.* 20 (1997) 207–216.
17. L.J. Cummings, Flow around a wedge of arbitrary angle in a Hele-Shaw cell. *Eur. J. Appl. Math.* 10 (1999) 547–560.
18. A.R. Kacimov and N.D. Yakimov, Moving phreatic surface in a porous slab: an analytical solution. *J. Engng. Math.* 40 (2001) 399–411.
19. A.R. Kacimov and Yu.V. Obnosov, Analytical determination of seeping soil slopes of a constant exit gradient. *Zeitschr. Angew. Math. Mech. (Z.A.M.M.)* 82 (2002) 363–376.
20. A.R. Kacimov, Yu.V. Obnosov and J. Perret, Phreatic surface from a near-reservoir saturated tongue. *J. Hydrol.* 296 (2004) 271–281.
21. Yu.V. Obnosov, Explicit solution of certain problem of R-linear conjugation for a regular triangular chess field. *Russian Math.* 38 (1994) 43–64.
22. A.R. Tsitskishvili, Methods of solution of a class of plane problems of the theory of filtration. In: V.N. Emikh (ed.), *Mathematical Models of Filtration and Their Applications*. Novosibirsk: Institute of Hydrodynamics (1999) (in Russian) pp. 177–188.
23. M. Abramowitz and I.A. Stegun, *Handbook of Mathematical Functions*. New York: Dover (1970) 1046 pp.
24. I.S. Gradshteyn and I. Ryzhik, *Tables of Integrals, Series and Products*. New York: Academic Press (1980) 1060 pp.
25. S. Wolfram, *Mathematica. A System for Doing Mathematics by Computer.* Redwood City: Addison-Wesley (1991) 961 pp.
26. O.D.L. Strack and M.I. Asgian, A new function for the use in the hodograph method. *Water Resour. Res.* 14 (1978) 1045–1058.
27. E.G. Youngs, An examination of computed steady-state water-table heights in unconfined aquifers: Dupuit-Forchheimer estimates and exact analytical results. *J. Hydrol.* 119 (1990) 201–214.
28. A.R. Kacimov, Unsaturated quasi-linear flow analysis in V-shaped domains. *J. Hydrol.* 279 (2003) 70–82.
29. A.R. Kacimov, M.M. Sherif, J.S. Perret and A. Al-Mushikhi. Sea water intrusion in an unconfined coastal aquifer on a catchment scale: modeling and field studies. *Hydrogeol. J.* (submitted, under review).
30. A.R. Kacimov and M.M. Sherif. Sea water intrusion into a confined aquifer with controlled pumping: analytical solution. *Water Resour. Res.* (submitted, under review).